International Geology Review, Vol. 49, 2007, p. 313–328.

Continuous Metamorphic Zircon Growth and Interpretation of U-Pb SHRIMP Dating: An Example from the Western Himalaya

MARY L. LEECH,[1]

Department of Geosciences, San Francisco State University, San Francisco, California 94132

S. SINGH, AND A. K. JAIN

Department of Earth Sciences, Indian Institute of Technology, Roorkee, 247667, India

Abstract

Ultrahigh-pressure (UHP) rocks in the northwest Himalaya are some of the youngest on earth, and allow testing of critical questions of UHP metamorphism and exhumation and the India-Asia collision. The Tso Morari Complex (TMC) is a UHP subduction-zone complex in eastern Ladakh in the western Himalaya, south of the Indus-Yarlung suture zone. U-Pb SHRIMP dating of zircon shows the TMC has a Proterozoic protolith, preserves a Pan-African magmatic history, and shows continuous metamorphic zircon growth during the Early to Middle Eocene, hence constraining the timing of collision, subduction, and exhumation in the western Himalaya. Zircon dating indicates that UHP metamorphism occurred at 53.3 ± 0.7 Ma, followed by 8 m.y. of continual zircon crystallization to amphibolite-facies metamorphic conditions at 45.2 ± 0.7 Ma. Similar continuous zircon growth during UHP metamorphism and through early exhumation to amphibolite-facies conditions occurs in other UHP subduction complexes, including the Sulu terrane, where coesite-bearing inclusions within dated zircon prove conclusively that zircon dates record UHP metamorphism. U-Pb SHRIMP dating of zircon for both the TMC and the Sulu belt demonstrate that zircon continues to crystallize at temperatures 400° ± 50°C based on $^{40}Ar/^{39}Ar$ dating yielding the same ages.

Introduction

THE TSO MORARI COMPLEX formed as a result of UHP metamorphism during subduction of the Indian subcontinent beneath Asia in the Early Eocene. The continent-continent collision is thought to have begun at 55 ± 1 Ma in the northwest Himalaya based on stratigraphy of collision-related sediments on both sides of the Indus-Yarlung suture zone (IYSZ) and a slowing of convergence rates (Klootwijk et al., 1992; Guillot et al., 2003). The UHP eclogites from Tso Morari, India, and Kaghan, Pakistan (e.g., Pognante and Spencer, 1991; Jain et al., 2003; Kaneko et al., 2003), are evidence that the leading edge of the entire northwestern part of the Indian continental margin was subducted beneath the Kohistan-Ladakh arc to a minimum of 90 km. Previously published age estimates for peak metamorphism for the TMC are based on Sm-Nd, Lu-Hf, and $U\text{-}Pb_{allanite}$ dating with significant errors (55 ± 7 Ma, 55 ± 12 Ma, and 55 ± 17 Ma, respectively; see de Sigoyer et al., 2000) and do not allow precise analysis of the geologic evolution in such a young mountain belt. Our U-Pb SHRIMP dating of zircons from the TMC better defines the ages of peak UHP and retrograde metamorphism, thus constraining the P-T-t path and exhumation history of the TMC, and helps resolve the timing of subduction and collision in the northwest Himalaya.

The UHP Tso Morari Complex

The TMC is a 100 × 50 km NW-SE–trending UHP eclogitic subduction zone complex in the eastern Ladakh area near the western syntaxis of the Himalaya, south of the Indus-Yarlung suture zone (Fig. 1). The TMC was first described by Berthelsen (1953), and subsequently mapped by Srikantia and Bhargava (1976); it is comprised of Proterozoic to Paleozoic quartzofeldspathic orthogneiss and metasedimentary rocks, Paleozoic intrusive granitoids, and small eclogite bodies and their retrogressed equivalents (e.g., de Sigoyer et al., 1997; 2000; Guillot et al., 1997; Girard and Bussy, 1999; Jain et al., 2003). The TMC is tectonically bound by the IYSZ along its entire northeastern margin and by the Tethyan sedimentary zone along its southwestern margin.

[1]Corresponding author; email: leech@sfsu.edu

0020-6814/07/925/313-16 $25.00

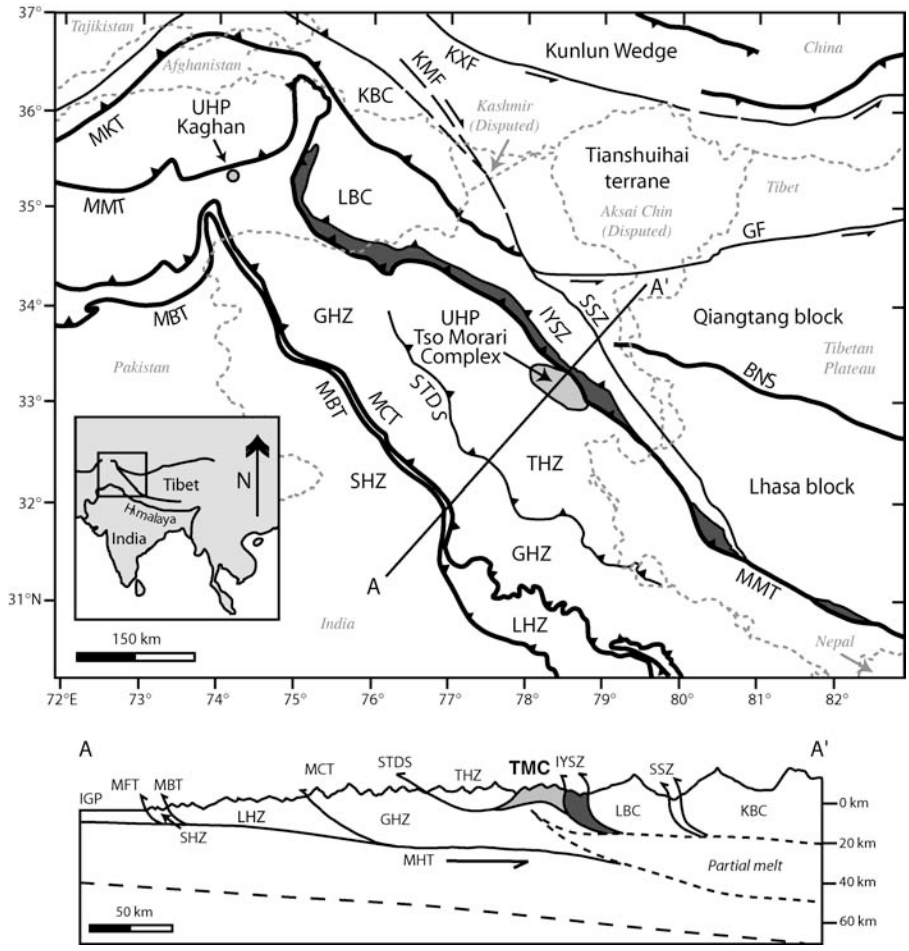

FIG. 1. Regional tectonic map of the western Himalaya showing the Tso Morari Complex (pale grey) and the Indus-Yarlung suture zone (dark grey) (adapted from de Sigoyer et al., 2000; Guillot et al., 2003; Jain et al., 2003; Lacassin et al., 2004). Simplified modern cross-section A-A' (modified after Jain et al., 2003; approximate location on map) shows the Tso Morari Complex in the footwall of the Indus-Yarlung suture zone and the ~10° modern subduction angle (true scale below sea level; topography is exaggerated). Abbreviations: BNS = Bangong-Nujiang suture; GF = Gozha fault; GHZ = Greater Himalayan zone; IGP = Indo-Gangetic plain; IYSZ = Indus-Yarlung suture zone; KBC = Karakoram batholith complex; KMF = Karakoram fault; KXF = Karakax fault; LBC = Ladakh batholith complex; LHZ = Lesser Himalayan zone; MBT = Main Boundary thrust; MCT = Main Central thrust; MHT = Main Himalayan thrust; MKT = Main Karakoram thrust; MMT = main mantle thrust; SHZ = Sub-Himalayan zone; SSZ = Shyok suture zone; STDS = South Tibetan detachment system; THZ = Tethyan Himalayan zone.

Sachan et al. (2001) first reported coesite inclusions in garnet from TMC eclogites. Peak P-T conditions for the TMC were 750° to 850°C and a minimum of 2.7 GPa based on conventional thermobarometric calculations, *Thermocalc* estimates (Powell and Holland, 1988), and the minimum pressure for coesite formation (Jain et al., 2003 and references therein). Retrograde HP eclogite-facies (2.0 GPa, 600°C) and amphibolite-facies metamorphism (1.3 GPa, 600°C) was followed by greenschist-facies metamorphism (0.4 GPa, 350°C) and final exhumation to the upper crust (Jain et al., 2003; Schlup et al., 2003; de Sigoyer et al., 2000). The P-T paths for Tso Morari metapelites and eclogites are similar, indicating they followed the same tectonometamorphic history (de Sigoyer et al., 1997). Table 1 shows

TABLE 1. Summary of Geochronologic Data for the Tso Morari Complex[1]

Rock type	Age (Ma)	Method	Mineral	P-T or T_c estimate	Reference
Proterozoic protolith ages					
Gneiss	748 ± 11–1744 ± 24	SHRIMP	Zircon		This study
Pan-African ages					
Granite	482 ± 1	U-Pb	Zircon		Girard and Bussy, 1999
Metagranite	479 ± 2	U-Pb	Zircon		Girard and Bussy, 1999
Gneiss	479 ± 2	U-Pb	Zircon		Girard and Bussy, 1999
Gneiss	462 ± 9–477 ± 10	SHRIMP	Zircon		This study
UHP eclogite-facies event				~800°C/≥2.9 GPa	
Eclogite?	55 ± 17	U-Pb	Allanite		de Sigoyer et al., 2000
Eclogite	55 ± 12	Lu-Hf	Grt-Omp-WR	600–750°C	de Sigoyer et al., 2000
Metapelite	55 ± 7	Sm-Nd	Grt-Gl-WR	600 ± 30°C	de Sigoyer et al., 2000
Gneiss	53.3 ± 0.7	SHRIMP	Zircon	≥900°C	This study
Eclogite-facies event				~600°C/2.0 GPa	
Gneiss	50.0 ± 0.6	SHRIMP	Zircon		This study
Amphibolite-facies event				~600°C/1.3 GPa	
Gneiss	53.8	$^{40}Ar/^{39}Ar$	Phengite	350-450°C	Schlup et al., 2003
Gneiss	51.1	$^{40}Ar/^{39}Ar$	Biotite	350°C	Schlup et al., 2003
Metapelite	48 ± 2	$^{40}Ar/^{39}Ar$	Phengite	350–450°C	de Sigoyer et al., 2000
Gneiss	47.5 ± 0.5	SHRIMP	Zircon		This study
Eclogite	47 ± 11	Sm-Nd	Grt-Amp-WR	600 ± 30°C	de Sigoyer et al., 2000
Metapelite	45.5 ± 4.4	Rb-Sr	Ap-Ph-WR		de Sigoyer et al., 2000
Gneiss	45.2 ± 0.7	U-Pb	Zircon		This study
Greenschist-facies event/late-stage exhumation					
Gneiss	34 ± 2–45 ± 2	FT	Zircon	~240°C/0.4 GPa	Schlup et al., 2003
Metapelite	31.1 ± 0.3	$^{40}Ar/^{39}Ar$	Muscovite	350°C	de Sigoyer et al., 2000
Metapelite	29.3 ± 0.3	$^{40}Ar/^{39}Ar$	Biotite	350°C	de Sigoyer et al., 2000
Metapelite	29 ± 0.4	$^{40}Ar/^{39}Ar$	Biotite	350°C	de Sigoyer et al., 2000
Gneiss	21 ± 3–26 ± 3	FT	Apatite	~110°C/0.2 GPa	Schlup et al., 2003

[1]See text for references for P-T and T_c estimates. Abbreviations: Amp = amphibole; Ap, = apatite; FT = fission-track; Grt, = garnet; Gl, = glaucophane; Ph = phengite; T_c, = closure temperature; WR = whole-rock.

P-T estimates based on thermobarometry and mineral closure temperature data.

Previous dating

de Sigoyer et al. (2000) reported an eclogitization age for the TMC of 55 Ma and syn-exhumation retrograde metamorphic events at ~47 Ma (amphibolite-facies) and 30 Ma (greenschist-facies) using multiple thermochronological techniques (Table 1); these ages are interpreted to record eclogite-facies metamorphism (2.0 ± 3 GPa, not UHP metamorphism) at about 55 Ma (55 ± 7 Ma, 55 ± 12 Ma, and 55 ± 17 Ma from Sm-Nd, Lu-Hf, and U-Pb on allanite, respectively) and overlap considerably with ages recording amphibolite-facies metamorphism (48 ± 2 Ma, 47 ± 11 Ma, and 45 ± 4 Ma from $^{40}Ar/^{39}Ar$, Sm-Nd, and Rb-Sr, respectively); this leaves open the question of exactly when UHP eclogite-facies metamorphism and the subsequent amphibolite-facies metamorphism occurred. The 55 Ma age for

peak metamorphism in the TMC is also the same date that is commonly cited for the timing of the initial India-Asia collision; UHP metamorphism could not have occurred at 55 Ma if the TMC was part of the Indian continent and, in fact, must be later.

The sometimes large analytical errors and discrepancies in mineral closure temperatures (T_c) for metamorphic ages shown in Table 1 require careful evaluation before interpretation. Sm-Nd ages record ~200°C below the peak UHP metamorphism temperatures for the TMC (Mezger et al., 1992). The Lu-Hf system may record similar temperatures to Sm-Nd, but results are quite variable; T_c can vary up to 150°C, from ~600°–750°C (Scherer et al., 2000; 2003). The T_c for U-Pb in zircon is about 1000°C (Cherniak and Watson, 2001, 2003), close to peak metamorphic temperatures for the TMC, so U-Pb SHRIMP dating of zircons presented here addresses the problem of these overlapping ages.

U-Pb Zircon SHRIMP Data

Dated zircons for this study are from two samples of quartzofeldspathic gneiss (T18 [78°16'40" E, 33°4'4" N] and T38 [78°21'33" E, 33°9'5" N]) from the UHP eclogitic country rock.

Sample preparation and analytical technique

A total of 78 analyses were completed for sample T38 and 14 analyses for sample T18 (see Table 2 for U-Th-Pb data for all analyses). Zircons were separated and mounted using standard sample-preparation methods for ion-microprobe analysis (Williams, 1998), and U-Pb SHRIMP analyses, data reduction using *Squid*, and plotting using *Isoplot* followed standard techniques (Williams, 1998; Ludwig, 1999). No morphologic or color differentiation was made during handpicking for the sample mount. Zircons include both subrounded and irregular-shaped grains that display clear core/mantle/rim zoning relationships under cathodoluminescence (CL) imaging (Fig. 2). SHRIMP analyses targeted rims that appeared to be metamorphic based on CL imaging (i.e., lack of oscillatory zoning, rounded grain morphology); analysis of zircon mantles and cores was performed for comparison and to establish different growth domains within the zircons. Pb/U ratios were calibrated with reference standard R33 (419 Ma; Black et al., 2004), which was analyzed after about every fourth unknown analysis. Zircons were analyzed using the SHRIMP-RG (-reverse geometry) at the Stanford-USGS Microanalysis Center. U-Th-Pb data for each ~30 μm spot were collected in five scans.

Results of dating

Figure 3 shows Tera-Wasserburg concordia diagrams for analyses from both samples; these concordia plots include some discordant data, and display mixing trends and discordance due to common Pb (all concordia plots show data uncorrected for common Pb). All weighted mean ages (95% confidence level) described for dating in this study are ^{207}Pb-corrected ^{206}Pb/^{238}U ages from concordant data or data within 1–2% of concordance; high U (>3000 ppm, Williams and Hergt, 2000, cited in Ireland and Williams, 2003), high common Pb, and discordant analyses were excluded from age calculations. Zircon rims yielding Eocene ages are only from sample T38 (Figs. 3A and 3B; Table 2). Out of 26 analyses that yielded Late Paleocene to Middle Eocene ages in sample T38, 11 were excluded from age calculations because they were more than 5% discordant. Both samples T18 and T38 give ~500–400 Ma ages from zircon cores and mantles (Figs. 3C and 3D). Thirteen analyses in T38 yielded ages in the Early Ordovician to Early Devonian; 11 of those analyses were concordant (2 were excluded because of high common Pb). Sample T18 yielded eight concordant analyses from the Middle Ordovician to the Early Devonian. Four zircon analyses in T38 indicate an inherited component with Late Proterozoic ages; two analyses were concordant at 1744 ± 24 Ma and 748 ± 11 Ma, corresponding to the Indian craton (DeCelles et al., 2000).

Pan-African Magmatism

Zircons from both samples T18 and T38 yielded ages between ~400 and 480 Ma (Fig. 4); it is likely these zircons record magmatism that was part of widespread late Pan-African magmatism along northern India (Singh and Jain, 2003). Girard and Bussy (1999) described late Pan-African magmatism ages (479 ± 2 to 482 ± 1 Ma) recorded by inherited zircons from the TMC using conventional U-Pb dating (Table 1). Pan-African granitic magmatism occurred in the Himalaya from 580 to 450 Ma, with an eastward progression over time (Girard and Bussy, 1999). The ~400–480 Ma ages from Tso Morari zircons were analyzed in zircon cores and mantles; the morphology of the zircons, the oscillatory zoning patterns, and Th/U ratios indicate that these ages result from igneous domains.

TABLE 2. SHRIMP U-Pb Analyses of Zircon from the Tso Morari Complex[1]

Spot	U (ppm)	Th (ppm)	Th/U	$^{204}Pb/^{206}Pb$	Common ^{206}Pb (%)	$^{238}U/^{206}Pb$*	$^{207}Pb/^{206}Pb$*	$^{207}Pb/^{235}U$#	$^{206}Pb/^{238}U$ Age† (Ma)
T18-1	1507	50	0.03	—	0.3	15.6384 ± 1.4103	0.0572 ± 1.0429	0.5046 ± 1.7540	398.3 ± 5.5
T18-2	2205	53	0.02	0.0000	0.2	15.5397 ± 1.3999	0.0565 ± 1.0951	0.4983 ± 1.7917	401.2 ± 5.5
T18-3	2539	66	0.03	0.0000	0.1	14.2586 ± 1.3952	0.0565 ± 0.8005	0.5419 ± 1.6441	436.5 ± 6.0
T18-4	2113	64	0.03	—	0.2	15.4847 ± 1.3970	0.0564 ± 0.8496	0.5020 ± 1.6351	402.6 ± 5.5
T18-5	2930	117	0.04	0.0000	0.8	36.6296 ± 1.7825	0.0557 ± 1.1411	0.2063 ± 2.2498	172.3 ± 3.1
T18-6	2093	46	0.02	0.0000	0.7	24.2033 ± 1.4127	0.0567 ± 1.1830	0.3146 ± 1.9713	259.3 ± 3.6
T18-7	2538	42	0.02	0.0000	0.6	21.9682 ± 1.4082	0.0567 ± 0.9742	0.3514 ± 1.7913	285.3 ± 4.0
T18-8	2770	29	0.01	—	0.7	27.1844 ± 1.4093	0.0564 ± 1.1034	0.2859 ± 1.7899	231.3 ± 3.2
T18-9	2828	74	0.03	0.0000	0.4	17.4286 ± 1.3899	0.0569 ± 0.7466	0.4471 ± 1.5986	358.3 ± 4.9
T18-10	705	37	0.05	—	0.1	14.7355 ± 1.4413	0.0562 ± 1.3091	0.5262 ± 1.9471	422.8 ± 6.0
T18-11	927	53	0.06	0.0000	1.3	44.1422 ± 1.6341	0.0594 ± 2.8614	0.1571 ± 7.7098	142.5 ± 2.3
T18-12	3350	95	0.03	0.0000	0.1	13.5219 ± 1.4113	0.0568 ± 0.9379	0.5727 ± 1.7499	459.6 ± 6.4
T18-13	1724	62	0.04	0.0000	0.2	14.5686 ± 1.4185	0.0571 ± 0.7813	0.5343 ± 1.6641	427.1 ± 5.9
T18-14	4776	78	0.02	0.0000	0.1	15.4304 ± 1.3860	0.0560 ± 0.5241	0.4973 ± 1.4880	404.2 ± 5.5
T38-1	1692	87	0.05	0.0000	0.2	8.8534 ± 1.509	0.0663 ± 1.6497	0.5565 ± 1.7732	448.8 ± 6.2
T38-2	525	148	0.28	0.0000	1.7	17.4707 ± 1.5559	0.0566 ± 2.0959	3.2778 ± 1.6132	1341.2 ± 19.3
T38-3	263	113	0.43	0.0003	0.5	131.1379 ± 1.6445	0.0525 ± 3.6255	0.9595 ± 3.0755	686.8 ± 10.1
T38-4	365	48	0.13	0.0004	0.4	25.0738 ± 1.4465	0.0569 ± 1.5013	0.3929 ± 5.0314	357.5 ± 5.5
T38-5	1411	10	0.01	0.0006	0.7	17.2124 ± 1.4711	0.0569 ± 1.5485	0.0453 ± 13.0028	48.6 ± 0.8
T38-6	1120	43	0.04	0.0000	0.7	13.4602 ± 1.3957	0.0568 ± 0.7569	0.3057 ± 2.2237	250.4 ± 3.6
T38-7	773	24	0.03	0.0001	0.4	135.4667 ± 2.1873	0.0542 ± 6.7433	0.4360 ± 2.5589	362.7 ± 5.3
T38-8	2058	34	0.02	0.0000	0.1	140.9974 ± 2.2457	0.0605 ± 6.6405	0.5767 ± 1.6054	461.6 ± 6.3
T38-9	408	5	0.01	0.0000	0.9	14.4942 ± 2.4568	0.0578 ± 6.2480	0.0552 ± 7.0892	47.0 ± 1.0
T38-10	794	7	0.01	0.0034	1.7	14.2310 ± 1.4221	0.0568 ± 1.1420	—	44.8 ± 1.0
T38-11	38	14	0.37	0.0006	0.3	15.3177 ± 1.4399	0.0567 ± 1.3542	0.4657 ± 13.8045	428.9 ± 10.5
T38-12	922	24	0.03	0.0000	0.1	14.7265 ± 1.3841	0.0713 ± 0.5055	0.5405 ± 1.9469	437.2 ± 6.1
T38-13	730	27	0.04	0.0001	0.2	13.0916 ± 1.5963	0.0576 ± 2.3918	0.4938 ± 2.3287	406.8 ± 5.8
T38-14	4155	30	0.01	0.0009	2.0	111.2412 ± 1.8618	0.1204 ± 7.1091	0.5367 ± 3.8399	415.3 ± 5.7
T38-15	186	58	0.31	0.0000	0.1	135.3161 ± 2.1997	0.0644 ± 6.3015	0.6071 ± 2.8756	473.9 ± 7.4

Table continues

TABLE 2. *Continued*

Spot	U (ppm)	Th (ppm)	Th/U	$^{204}Pb/^{206}Pb$	Common ^{206}Pb (%)	$^{238}U/^{206}Pb*$	$^{207}Pb/^{206}Pb*$	$^{207}Pb/^{235}U^{\#}$	$^{206}Pb/^{238}U$ Age† (Ma)
T38-16	580	77	0.13	0.0062	9.3	13.4268 ± 1.5201	0.0583 ± 1.1435	—	52.4 ± 1.3
T38-17	508	2	0.00	0.0025	2.2	18.5901 ± 1.4025	0.0568 ± 1.2363	0.0263 ± 50.7294	46.4 ± 1.1
T38-18	1396	23	0.02	0.0000	0.3	171.5470 ± 2.7355	0.0990 ± 6.7509	0.5828 ± 2.1609	461.9 ± 6.9
T38-19	1998	48	0.02	0.0000	0.4	65.9398 ± 1.8869	0.2454 ± 2.5881	0.4131 ± 1.9782	336.3 ± 4.7
T38-20	529	7	0.01	0.0120	6.6	118.7748 ± 2.1319	0.0581 ± 6.2166	—	35.0 ± 1.1
T38-21	361	18	0.05	0.0158	25.0	87.5273 ± 1.7442	0.1340 ± 14.2193	—	72.9 ± 3.4
T38-22	493	4	0.01	0.0030	1.4	131.6984 ± 2.1081	0.0567 ± 10.0734	—	53.3 ± 1.2
T38-23	500	38	0.08	0.0051	10.9	122.6140 ± 2.0048	0.0708 ± 5.1325	0.0864 ± 47.8656	65.3 ± 2.3
T38-24	424	1	0.00	0.0000	1.2	8.1187 ± 1.5489	0.0651 ± 1.7870	0.0594 + 10.2917	48.2 ± 1.1
T38-25	507	3	0.01	0.0028	3.0	3.2254 ± 1.4201	0.1051 ± 0.5420	0.0301 ± 55.9327	50.8 ± 1.1
T38-26	178	130	0.73	0.0001	0.1	12.9543 ± 1.4597	0.0566 ± 1.5690	1.0764 ± 2.5375	748.0 ± 11.3
T38-27	489	188	0.38	0.0000	-0.2	123.4885 ± 1.9745	0.0695 ± 4.9930	4.4758 ± 1.5354	1743.7 ± 24.2
T38-28	448	53	0.12	0.0000	0.0	136.3644 ± 2.1528	0.0622 ± 6.1108	0.5904 ± 2.4182	479.4 ± 6.9
T38-29	370	2	0.01	0.0009	2.8	118.4879 ± 2.1024	0.0705 ± 5.5458	0.0620 ± 10.1119	50.5 ± 1.0
T38-30	599	3	0.00	0.0000	1.9	92.6446 ± 1.9171	0.2682 ± 2.8124	0.0629 ± 6.4790	46.2 ± 1.0
T38-31	440	45	0.10	0.0028	3.0	14.1134 ± 0.3652	0.0571 ± 1.2060	0.0308 ± 80.1297	52.6 ± 1.2
T38-32	301	9	0.03	0.0203	27.9	11.7206 ± 0.3992	0.1285 ± 1.0672	—	50.0 ± 2.7
T38-33	410	33	0.08	0.0000	0.1	20.9361 ± 0.5469	0.0577 ± 1.1332	0.5499 ± 1.3535	440.6 ± 1.6
T38-34	318	65	0.21	0.0047	8.5	59.6268 ± 0.3301	0.0548 ± 1.3428	0.6443 ± 18.3866	482.6 ± 6.1
T38-35	849	45	0.05	0.0004	0.7	53.7913 ± 0.4935	0.0589 ± 2.2335	0.3417 ± 2.8917	298.8 ± 1.6
T38-36	1475	34	0.02	0.0002	0.3	134.3868 ± 2.3610	0.1864 ± 21.1838	0.1205 ± 2.4199	106.4 ± 0.4
T38-37	653	4	0.01	0.0003	0.5	131.6593 ± 0.9127	0.0731 ± 3.3954	0.1387 ± 4.9587	117.2 ± 0.6
T38-38	562	8	0.01	0.0039	7.0	15.6648 ± 0.3388	0.0583 ± 1.1535	0.0679 ± 72.0415	47.2 ± 0.5
T38-39	562	8	0.01	0.0077	7.0	126.1916 ± 1.0665	0.0628 ± 2.6413	—	47.2 ± 0.5
T38-40	586	267	0.47	0.0005	1.0	31.4252 ± 0.5479	0.0587 ± 3.4208	0.4393 ± 5.0313	397.2 ± 1.4
T38-41	961	2	0.00	0.0016	3.0	150.3122 ± 0.9567	0.0628 ± 3.8523	0.0404 ± 19.4544	49.9 ± 0.7
T38-42	384	19	0.05	0.0009	1.6	125.1164 ± 1.1462	0.0714 ± 9.3085	0.1980 ± 8.6671	199.8 ± 1.2
T38-43	538	8	0.01	0.0022	4.1	133.3284 ± 0.9303	0.0529 ± 4.0177	0.0254 ± 38.0814	41.9 ± 0.4
T38-44	336	1	0.00	0.0015	2.8	123.0497 ± 0.9423	0.0961 ± 3.0535	0.0532 ± 21.1635	49.8 ± 0.7
T38-45	419	2	0.00	0.0006	1.1	87.6734 ± 0.8520	0.0584 ± 3.4805	0.0446 ± 12.1739	47.8 ± 0.5

T38-46	371	1	0.00	0.0037	6.8	12.8848 ± 0.3296	0.0576 ± 1.0683	0.0413 ± 37.3453	49.1 ± 0.6
T38-47	348	1	0.00	0.0004	0.7	124.6407 ± 0.9025	0.0754 ± 5.7392	0.0824 ± 7.3547	72.1 ± 0.6
T38-48	514	30	0.06	0.0000	0.0	63.0556 ± 0.6498	0.0604 ± 2.5458	0.6146 ± 1.1331	481.3 ± 1.6
T38-49	872	7	0.01	0.0067	12.2	69.1642 ± 0.8252	0.0704 ± 3.0476	—	49.7 ± 0.6
T38-50	472	12	0.03	0.0010	1.9	114.7299 ± 0.7298	0.0604 ± 2.9250	0.0961 ± 11.0007	99.9 ± 0.7
T38-51	390	60	0.16	0.0021	3.7	63.0724 ± 1.2211	0.0598 ± 2.2571	0.0758 ± 25.0172	90.0 ± 0.8
T38-52	1164	6	0.00	0.0013	2.3	51.5326 ± 0.5659	0.0561 ± 3.0110	0.0482 ± 14.8285	55.0 ± 0.4
T38-53	1359	16	0.01	0.0025	4.5	122.4100 ± 1.0409	0.0762 ± 7.1467	0.0457 ± 38.2616	99.9 ± 1.2
T38-54	540	19	0.04	0.0007	1.2	103.0441 ± 1.3324	0.2918 ± 6.5428	0.1221 ± 8.5914	122.7 ± 0.7
T38-55	477	8	0.02	0.0038	6.8	139.0900 ± 0.8572	0.0649 ± 3.3765	—	50.6 ± 0.7
T38-56	430	10	0.02	0.0208	37.6	130.8656 ± 0.9004	0.1066 ± 3.0644	—	43.7 ± 2.8
T38-57	530	2	0.00	0.0029	5.3	117.8033 ± 0.6578	0.0643 ± 2.6103	0.0186 ± 60.6476	45.2 ± 0.4
T38-58	555	5	0.01	0.0076	13.7	68.7304 ± 0.7011	0.0623 ± 2.7119	—	45.5 ± 0.6
T38-59	836	5	0.01	0.0029	5.3	23.8414 ± 1.2700	0.0566 ± 1.3510	0.0220 ± 57.5181	53.3 ± 0.4
T38-60	510	2	0.00	0.0029	5.2	46.9308 ± 1.1933	0.0716 ± 2.3787	0.0342 ± 66.6467	91.5 ± 0.7
T38-61	831	40	0.05	0.0005	1.0	72.9258 ± 0.7315	0.0675 ± 2.9066	0.2769 ± 4.8455	263.3 ± 3.3
T38-62	408	16	0.04	0.0020	3.6	66.5008 ± 0.8679	0.4692 ± 5.0632	0.1186 ± 20.0913	132.1 ± 1.7
T38-63	577	6	0.01	0.0020	3.6	105.5547 ± 0.8432	0.0701 ± 3.1675	0.0684 ± 23.1249	85.7 ± 0.7
T38-64	665	12	0.02	0.0269	48.5	66.7073 ± 0.9952	0.1099 ± 7.3660	—	46.7 ± 6.7
T38-65	586	12	0.02	0.0032	5.7	64.2328 ± 1.0008	0.0669 ± 2.8173	0.0266 ± 62.9750	59.1 ± 0.6
T38-66	406	2	0.00	0.0131	23.6	90.9037 ± 0.9429	0.0834 ± 3.2342	—	88.7 ± 1.6
T38-67	651	9	0.01	0.0005	0.8	152.9934 ± 1.4226	0.0677 ± 4.9134	0.1280 ± 5.9391	97.3 ± 1.0
T38-68	418	56	0.14	0.0025	4.5	25.8752 ± 0.5559	0.0623 ± 2.0052	0.0674 ± 24.5217	67.4 ± 0.8
T38-69	396	7	0.02	0.0045	8.1	25.8893 ± 0.5119	0.0592 ± 1.8867	—	40.9 ± 0.6
T38-70	350	120	0.35	0.0020	3.6	33.0598 ± 0.8019	0.0718 ± 1.7593	0.1672 ± 25.0025	241.1 ± 1.4
T38-71	347	19	0.05	0.0005	1.0	62.0157 ± 0.6289	0.0645 ± 2.3934	0.2682 ± 6.0081	241.9 ± 1.3
T38-72	632	40	0.06	0.0021	3.8	109.7761 ± 1.6477	0.1460 ± 8.9024	0.1614 ± 18.8451	187.0 ± 1.6
T38-73	570	16	0.03	0.0011	2.0	63.3291 ± 0.6064	0.0628 ± 3.2410	0.1046 ± 6.7884	101.0 ± 0.7
T38-74	675	44	0.07	0.0245	44.2	26.9720 ± 0.4852	0.0574 ± 1.6141	—	51.4 ± 1.5
T38-75	634	8	0.01	0.0046	8.4	77.7867 ± 0.9407	0.0940 ± 8.6446	—	99.2 ± 0.7
T38-76	524	10	0.02	0.0002	0.3	22.5382 ± 0.3730	0.0838 ± 2.7228	0.2794 ± 2.0116	232.8 ± 1.2
T38-77	488	7	0.01	0.0074	13.4	—	—	—	77.7 ± 1.2
T38-78	975	26	0.03	0.0016	2.9	—	—	0.3579 ± 9.8150	269.0 ± 1.8

[1]1σ error unless noted otherwise; * = uncorrected; error given as percentage; # = corrected for ^{204}Pb; error given as percentage; † = corrected for ^{207}Pb.

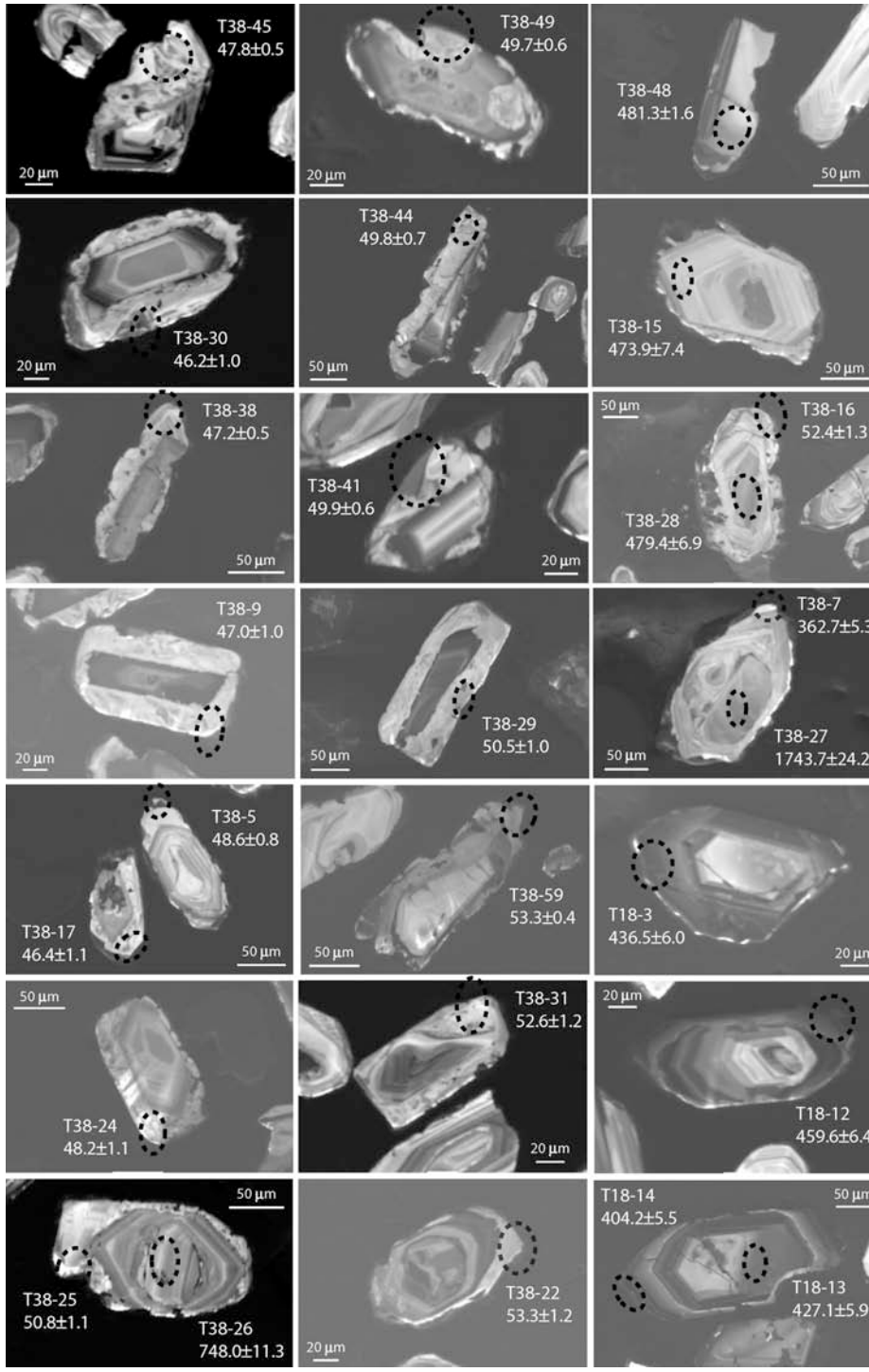

FIG. 2. Cathodoluminescence images of Tso Morari zircons showing individual SHRIMP analysis spots (U-Pb dating and REE analyses). All zircon rims yielding Eocene metamorphism ages, and representative zircon mantles and cores with Pan-African or protolith ages, are shown. Sample and spot numbers are listed with ^{207}Pb-corrected ages (in Ma).

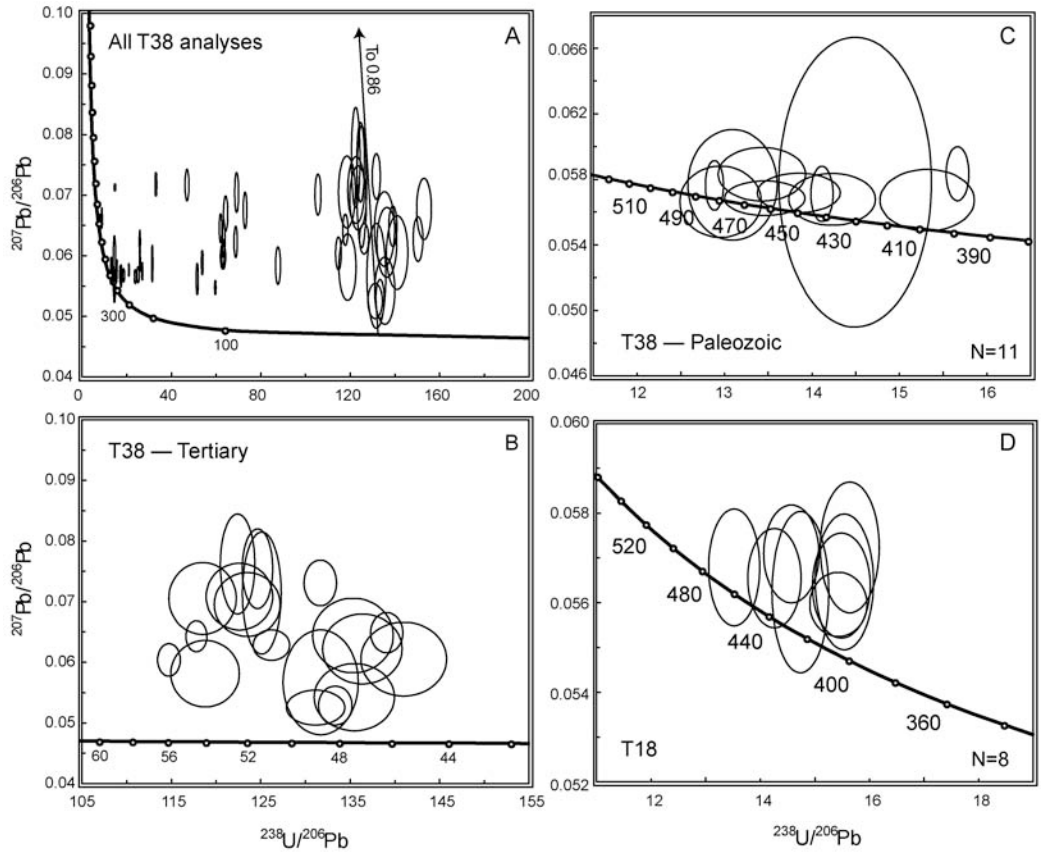

FIG. 3. Tera-Wasserburg concordia diagrams showing U-Pb SHRIMP data for samples T18 and T38 from the Tso Morari Complex. A. All analyses for sample T38. B. Near-concordant Tertiary analyses for T38. C. Concordant and near-concordant Paleozoic zircon ages. D. Concordant and near-concordant analyses for T18. Data are uncorrected for common Pb (error ellipses are 2σ); all data shown are greater than 95% concordant, and analyses high in common Pb were excluded. Discordance was estimated by using a mixing line between the common Pb ratio ($^{207}Pb/^{206}Pb = 0.86$) and the concordia line.

Sample T38 yields 11 concordant analyses with corrected ages ranging from 397.2 ± 1.4 to 481.3 ± 1.6 Ma; weighted mean averages yield several age groups (based on cumulative probability curves) at 480.9 ± 3.0 Ma (three spots) and 440.6 ± 2.9 Ma (four spots), and a single spot at 397.2 ± 1.4 Ma. Eight concordant analyses in sample T18 have corrected ages ranging from 398.3 ± 5.5 to 459.6 ± 6.4 Ma; best ages include weighted mean averages of 402.7 ± 6.2 Ma (three spots) and 424.9 ± 8.3 Ma (two spots), and a single spot age of 459.6 ± 6.4 Ma.

The 480.9 ± 3.0 Ma weighted mean average age in T38 corresponds well to the 479 ± 2 to 482 ± 1 Ma ages from Girard and Bussy (1999) (Table 1). Several of the younger Pan-African ages with reasonably small analytical errors (see Table 4 in Girard and Bussy, 1999) fall within the range of 460–470 Ma and correspond to the ages seen in both T18 and T38. The lower limits of errors on ages for Pan-African magmatism reach 398 Ma (Girard and Bussy, 1999, and references therein), therefore the younger ages seen in both T18 and T38 from 397 to 449 Ma may represent very late stage Pan-African magmatism.

Eocene Zircon Growth

Nineteen concordant zircon analyses from sample T38 yield ages from a 10 m.y. period in the Early to Middle Eocene from about 55 to 45 Ma (Fig. 4A,

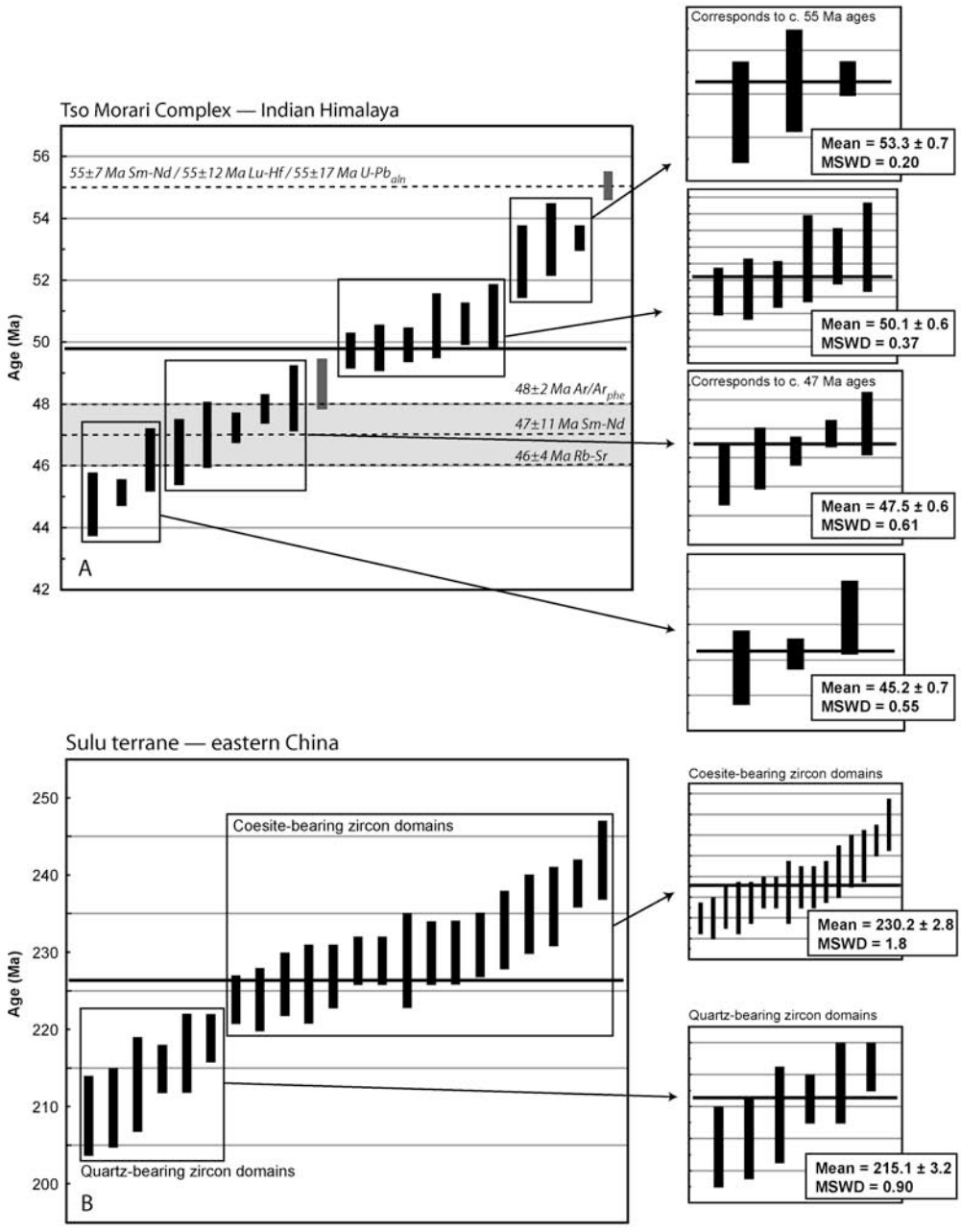

FIG. 4. Weighted mean age plots for the Tso Morari Complex (A) and the Sulu terrane (B) showing continuous metamorphic zircon growth from UHP conditions through early exhumation. A. Four "snapshots" of metamorphic zircon growth at ~53, 50, 47, and 45 Ma correspond to—and are bracketed by—multiple thermochronometers (see Table 1). B: A similar example of continuous metamorphic zircon growth from the Sulu terrane, China (from Liu et al., 2004) wherein the older ages are from coesite-bearing zircon domains, and the younger ages correspond to quartz-bearing zircon domains. All weighted mean ages (95% confidence level) described for dating in this study are ^{207}Pb-corrected ^{206}Pb/^{238}U ages from concordant data or data within 1–2% of concordance. High U, high common Pb, and discordant analyses were excluded from age calculations.

Table 2); morphological and CL characteristics, and U-Th-Pb concentrations do not allow us to distinguish zircons from each of these three age groups (Figs. 2 and 3; Table 2). Analyses that yielded Eocene ages were from thin, bright rims (under CL) with darker cores/mantles; these metamorphic rims had very low Th/U ratios (<0.14 with most <0.02). There are only rare inclusions in these rims, and included minerals do not allow for thermobarometric estimates. Most metamorphic rims were too thin to yield sufficient U for analysis or the beam overlapped into older growth domains within the zircon and yielded an older apparent (mixed) age.

Because of the small amount of radiogenic Pb in Tertiary zircon, $^{207}Pb/^{206}Pb$ and $^{207}Pb/^{235}U$ ages determined by the ion microprobe have high uncertainties and cannot be use to evaluate discordance. However, assuming common Pb is the most significant factor in producing discordance toward a common-Pb $^{207}Pb/^{206}Pb$ ratio (0.86 ± 0.6; Cumming and Richards, 1975), then a common-Pb correction provides acceptable estimates of true ages (DeGraaff-Surpless et al., 2003). This is a reasonable assumption for zircons in this study because the data that plot above concordia fit a mixing line toward a $^{207}Pb/^{206}Pb$ ratio for common Pb and do not fit a mixing line toward older ages (Figs. 3A and 3B).

The Tera-Wasserburg concordia diagram provides a graphical estimate of discordance in young zircon grains by showing uncorrected $^{207}Pb/^{206}Pb$ ratios plotted against uncorrected $^{238}U/^{206}Pb$ ratios (Fig. 3B). Discordance of Eocene grains was estimated by determining where data fall on a mixing line from the common-Pb value through the data to concordia. Eocene zircon data shown in Figure 3B only includes grains more than 95% concordant; analyses with high common Pb were excluded.

REE Analyses of Triassic Zircon Domains

Rare-earth-element (REE) data were collected using the SHRIMP-RG in the same analysis spots for which U-Pb dating was done in an attempt to distinguish between eclogite-facies zircon growth and lower-grade metamorphic zircon growth.

Analytical technique

The lack of well-characterized zircon crystals for REE calibration standards requires calibration to other REE and zircon standards. For our analyses, we calibrated to: NIST SRM 611 and NIST SRM 613 (REE-spiked) glasses; SL13 standard zircon (REE concentrations based on SL13-LA-CH in Hoskin, 1998); and CZ3 (U-concentration standard). NIST glasses and SL13 zircon were analyzed at the beginning and end of the SHRIMP session. Rare-earth data were collected in three scans, with the CZ3 standard repeated after every twelfth analysis; multiple CZ3 and SL13 standards were run before and after each sample. Details of data reduction were as described by Hoskin (1998); data were normalized to the chondrite values of McDonough and Sun (1995).

Summary and interpretation of REE data

Sample T38 was analyzed for REEs and show consistent patterns of depleted LREEs with slight negative Eu anomalies and enriched HREEs with respect to MREEs. Figure 5 shows REE patterns for zircons yielding Eocene ages (see Fig. 2, Table 2). Although patterns for all analyses are broadly similar, those REE patterns for the older dates (~53 Ma) are more enriched in the LREEs, specifically La and Ce, with concentrations roughly two orders of magnitude higher, whereas La and Ce concentrations for younger ages are much lower and more variable.

Zircon growing in the presence of garnet should show a depleted HREE pattern because garnet preferentially incorporates HREEs; in contrast, magmatic zircon grown in the presence of plagioclase should have elevated HREEs and a negative Eu anomaly (example in Fig. 5; Hermann et al., 2001; Rubatto, 2002; Rubatto and Hermann, 2003). Our age and REE data for zircons are from quartzofeldspathic gneisses that have abundant feldspar and only rare to minor garnet; consequently the REE patterns are generally consistent with zircon growing in association with feldspar. These REE patterns do not rule out zircon crystallization at eclogite-facies in a largely garnet-free rock, but may reflect zircon growth under amphibolite-facies conditions for some zircons based on our interpretation of the age data for these samples below.

Interpreting UHP versus Retrograde Zircon Crystallization Ages

Sorting the Eocene-age data by age yields what appears to be continuous zircon crystallization from ~55 to 45 Ma (Fig. 4A). It is inappropriate to estimate the timing of peak metamorphism by calculating a weighted mean age from these 19 analyses spanning 10 m.y.; this would result in a young

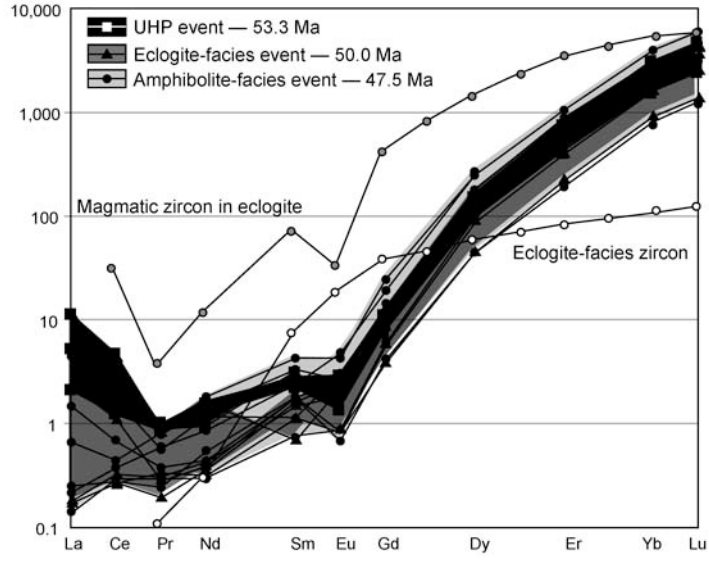

FIG. 5. Chondrite-normalized (McDonough and Sun, 1995) REE patterns of zircons yielding Tertiary U-Pb ages for sample T38. Two typical patterns for magmatic zircon and eclogite-facies zircon (from Rubatto and Hermann, 2003) are shown for comparison.

apparent age with a large amount of uncertainty (49.7 ± 1.6 Ma; MSWD = 26). We separate these data into four age groups (Fig. 4A) with overlapping 1σ error bars, and include the maximum number of analyses that yield ages with small errors and low MSWD values: 53.3 ± 0.7 Ma (MSWD = 0.20), 50.1 ± 0.6 Ma (MSWD = 0.37), 47.5 ± 0.6 Ma (MSWD = 0.61), and 45.2 ± 0.7 Ma (MSWD = 0.55). These ages are effectively snapshots in time during continuous metamorphism from UHP conditions through early exhumation.

Our Eocene U-Pb SHRIMP ages correspond well to—and are in part bracketed by—existing thermochronometric data for peak and retrograde metamorphic events in the TMC at ~55 ± 11 Ma and 47 ± 3 Ma, respectively (de Sigoyer et al., 2000; Table 1). We interpret the oldest Eocene age (53.3 ± 0.7 Ma) to date UHP metamorphism in the TMC because it corresponds to three different radiometric dating systems that shows peak metamorphism took place at ~55 Ma (de Sigoyer et al., 2000; Fig. 4A, Table 1). The 47.5 ± 0.6 Ma age from this study is equivalent to the 45–48 Ma ages obtained by de Sigoyer et al. (2000) for the amphibolite-facies retrograde metamorphism using $^{40}Ar/^{39}Ar$, Rb-Sr, and Sm-Nd dating methods. Well-established $^{40}Ar/^{39}Ar$ closure temperatures exist for biotite, muscovite, and phengite, ranging from 350 to 400° ± 50°C (McDougall and Harrison, 1999); these ages therefore record syn-exhumation cooling in UHP terranes.

The 50.0 ± 0.6 Ma age, intermediate between the UHP and the amphibolite-facies metamorphism (Fig. 4A, Table 1), corresponds to metamorphism that is recorded by several thermobarometric calculations (see Guillot et al., 1997; de Sigoyer et al., 2000; Jain et al., 2003) and falls on the exhumation path between the UHP and amphibolite-facies events (Fig. 6). Similar to other UHP terranes (e.g., Leech and Willingshofer, 2004), standard thermobarometric calculations (using Fe-Mg exchange in garnet and omphacite [de Sigoyer et al., 2004]) record retrograde P-T conditions rather than peak metamorphic conditions; temperature estimates will also be too low if the estimated pressure used in the calculation is too low (de Sigoyer et al., 2004 uses 2.0–2.5 GPa despite the occurrence of coesite). Analytical errors were too large with previous dating methods to distinguish this metamorphic event. The final group of ages at 45.2 ± 0.7 Ma must record the lowest-temperature zircon growth (~350–450°C, corresponding to the lower limit of closure temperatures in phengite for the $^{40}Ar/^{39}Ar$ system).

Abundant examples exist of low-temperature zircon crystallization, including amphibolite-facies zircon growth in diamondiferous UHP rocks from the Kokchetav massif (Hermann et al., 2001). Similar

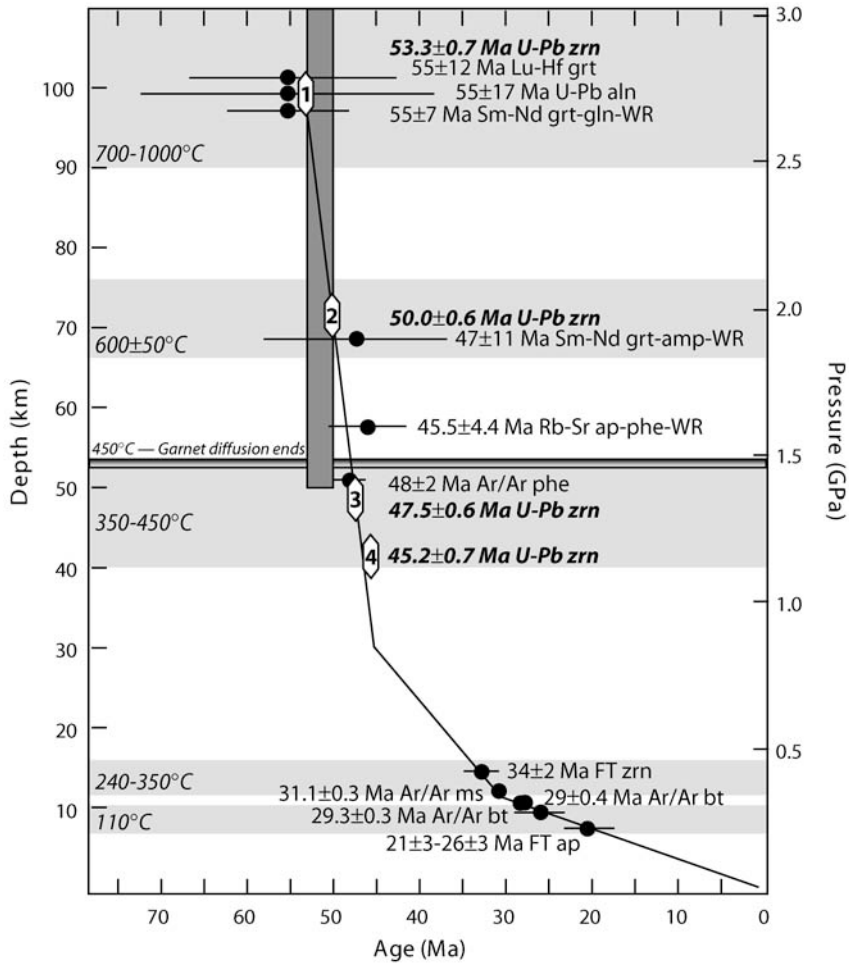

FIG. 6. Age-depth diagram showing conditions for the Tso Morari Complex during UHP metamorphism, and subsequent exhumation with results of various radiometric dating methods (see Table 1; de Sigoyer et al., 2000, Schlup et al., 2003; Leech et al., 2005) plotted in appropriate temperature ranges for those methods (modified after Fig. 17 in Massonne and O'Brien, 2003). The exhumation P-T-t path shown is modified from de Sigoyer et al. (2000) to account for the more recent discovery of coesite and other mineralogical evidence for UHP metamorphism (Sachan et al., 2001, 2004; Mukherjee and Sachan, 2003; Leech et al., 2006a). The vertical bar represents a 3 m.y.–wide period corresponding to the garnet diffusion modeling of Konrad-Schmolke et al. (2005) and Massonne and O'Brien (2003), stopping at about 450°C, at which point garnet diffusion ends; this 3 m.y.–period fits all high- and intermediate-temperature geochronometry within error. White symbols correspond to U-Pb SHRIMP dating of zircon from this study as outlined in Figure 4A.

to the multiple stages of Eocene zircon growth described in this study, Hermann et al. (2001) demonstrated that coesite-and diamond-bearing zircon (their Domain 2) looks identical under CL to growth domains recording upper amphibolite- to granulite-facies zircon growth (their Domain 3). U-Th-Pb concentrations for Domains 2 and 3 in Kokchetav zircons are indistinguishable, just as are U-Th-Pb concentrations in TMC zircon rims.

Continuous Metamorphic Zircon Growth

In the Sulu terrane, China, coesite-bearing zircon domains (cores and mantles) unquestionably yield the timing for UHP metamorphism, whereas younger quartz-bearing zircon rims record retrograde zircon growth (Liu et al., 2004). Sorting the Sulu U-Pb data (from Liu et al., 2004) by age shows the same continuum of zircon growth from UHP to

retrograde metamorphic conditions (Fig. 4B). Leech et al. (2006b) demonstrate that U-Pb ages on different zircons from the same area, but lacking UHP index mineral inclusions, record the same span of ages for peak and retrograde zircon growth as described by Liu et al. (2004); $^{40}Ar/^{39}Ar$ dating records retrograde metamorphism in the same rocks (Webb et al., 2006). Similar examples of continuous metamorphic zircon growth are seen in UHP rocks from eastern Greenland (McClelland et al., in press) and the Ural Mountains, Russia (Beane and Leech, in press).

Comparing our U-Pb SHRIMP dating of zircon to results from several other radiometric dating systems indicates that metamorphic zircon growth can continue essentially uninterrupted from UHP conditions (ca. ≤1000°C) through exhumation to the mid-crust at significantly lower temperatures (ca. 350–450°C); this is a reliable method to help interpret U-Pb age dating when internal evidence is lacking (see the section on Eocene Zircon Growth).

A new model for diffusion in garnet (Konrad-Schmolke et al., 2005) from the Tso Morari Complex describes a rapid exhumation period from peak through retrograde metamorphism to no more than 3 m.y., ending with garnets cooling below about 450°C when measurable diffusion in garnet ends. The results of dating from this study and multiple intermediate- to high-temperature geochronometers (≥450°C) reported in de Sigoyer et al. (2000) all fit, within error, this 3 m.y. period from 53 to 50 Ma. Figure 6 illustrates how zircon continued to grow from peak metamorphic conditions through much lower temperatures during exhumation (to about 400°C).

Timing of UHP Metamorphism and the India-Asia Collision

The timing of UHP metamorphism (53.3 ± 0.7 Ma) in the TMC is ~2 m.y. younger than estimates for the timing of the initial collision between India and Asia at 55 ± 1 Ma (see discussion in Guillot et al., 2003 and Leech et al., 2005). In order to reconcile the short period of time available for Tso Morari protoliths to enter the subduction zone along the leading edge of the Indian continent and then to recrystallize under UHP conditions, subduction must have been vertical. Leech et al. (2005) presented a subduction model using this U-Pb SHRIMP dating to quantify the timing and angle of subduction; the model considers the geometry of a subduction zone, accounting for the strength of the continental lithosphere, and recalculates the timing of the initial collision between continental India and Asia from 55 Ma to 57 Ma. Zircon geochronology using the precision of SHRIMP and other ion microprobe analyses have applicability beyond constraining complex metamorphic histories; tectonic models of continental collision, subduction, and exhumation result from careful U-Pb dating (e.g., Guillot et al., 2004, 2006; Leech et al., 2005) and give insight into much larger scale processes.

Acknowledgments

This work was supported in part by U.S. NSF-EAR 0003355 to J. G. Liou. Field work was funded by a NSF-AAAS WISC program travel grant and the Department of Science and Technology (DST) of India under its HIMPROBE program. We are grateful to Kailash Chandra and T.K. Ghosh for use of the EPMA facilities at the Institute Instrumentation Centre, IIT Roorkee. We thank Joe Wooden and Jeremy Hourigan (now at University of California at Santa Cruz) for help in the Stanford/USGS SHRIMP lab, Ruth Zhang for help analyzing samples, and Kathy DeGraaff-Surpless for help with data analysis. Laura Webb (Syracuse University) helped to interpret $^{40}Ar/^{39}Ar$ data. Thanks also to George Chang and Guenther Walther in Stanford's Statistics Department. James Crowley and one anonymous reviewer provided several suggestions on an early version of this manuscript that helped to improve this work.

REFERENCES

Beane, R., and Leech, M., in press, The Maksyutov Complex: The first UHP terrane 40 years later, *in* Cloos, M., Carlson, B., Gilbert, C., Liou, J. G., and Sorenson, S., eds., Convergent margin terranes and associated regions: A volume in honor of W.G. Ernst: Geological Society of America Special Paper.

Berthelsen, A., 1953, On the geology of the Rupshu district, northwest Himalaya: Meddelelser fra Dansk Geologisk Førening, v. 12, p. 350–414.

Black, L. P., Kamo, S. L., Allen, C. M., Davis, D. W., Aleinikoff, J. N., Valley, J. W., Mundil, R., Campbell, I. H., Korsch, R. J., Williams, I. S., and Foudoulis, C., 2004, Improved $^{206}Pb/^{238}U$ microprobe geochronology by the monitoring of trace-element-related matrix zircon standards: Chemical Geology, v. 205, p. 115–140.

Cherniak, D. J., and Watson, E. B., 2001, Pb diffusion in zircon: Chemical Geology, v. 172, p. 5–24.

Cherniak, D. J., and Watson, E. B., 2003, Diffusion in zircon: Reviews in Mineralogy and Geochemistry, v. 53, p. 113–143 [doi: 10.2113/0530113].

Cumming, G. L., and Richards, J. R., 1975, Ore lead isotope ratios in a continuously changing Earth: Earth and Planetary Science Letters, v. 28, p. 155–171.

DeCelles, P. G., Gehrels, G. E., Quade, J., LaReau, B., and Spurlin, M., 2000, Tectonic implications of U-Pb zircon ages of the Himalayan orogenic belt in Nepal: Science, v. 288, p. 497–499.

DeGraaff-Surpless, K., Mahoney, J. B., Wooden, J. L., and McWilliams, M. O., 2003, Lithofacies control in detrital zircon provenance studies: Insights from the Cretaceous Methow basin, southern Canadian Cordillera: Geological Society of America Bulletin, v. 115, p. 899–915.

de Sigoyer, J., Chavagnac, V., Blichert-Toft, J., Villa, I. M., Luais, B., Guillot, S., Cosca, M., and Mascle, G., 2000, Dating the Indian continental subduction and collisional thickening in the northwest Himalaya: Multichronology of the Tso Morari eclogites: Geology, v. 28, p. 487–490.

de Sigoyer, J., Guillot, S., and Dick, P., 2004, Exhumation of the ultrahigh-pressure Tso Morari unit in eastern Ladakh (NW Himalaya): A case study: Tectonics, v. 23, 18 p. [doi: 10.1029/2002TC001492].

de Sigoyer, J., Guillot, S., Lardeaux, J.-M., and Mascle, G., 1997, Glaucophane-bearing eclogites in the Tso Morari dome (eastern Ladakh, NW Himalaya): European Journal of Mineralogy, v. 9, p. 1073–1083.

Girard, M., and Bussy, F., 1999, Late Pan-African magmatism in Himalaya: New geochronological and geochemical data from the Ordovician Tso Morari metagranites (Ladakh, NW India): Schweizerische Mineralogische und Petrographische Mitteilungen, v. 79, p. 399–418.

Guillot, S., de Sigoyer, J., Lardeaux, J. M., and Mascle, G., 1997, Eclogitic metasediments from the Tso Morari area (Ladakh, Himalaya): Evidence for continental subduction during India-Asia convergence: Contributions to Mineralogy and Petrology, v. 128, p. 197–212.

Guillot, S., Garzanti, E., Baratoux, D., Marquer, D., Mahéo, G., and de Sigoyer, J., 2003, Reconstructing the total shortening history of the NW Himalaya: Geochemistry, Geophysics, Geosystems, v. 4 [doi: 10.1029/2002GC000484].

Guillot, S., Replumaz, A., Hattori, K. H., and Strzerzynski, P., 2006, Initial geometry of western Himalaya inferred from ultra-high pressure metamorphic evolution: Journal of Asian Earth Sciences, v. 26, p. 139.

Guillot, S., Replumaz, A., and Strzerzynski, P., 2004, Himalayan ultrahigh pressure rocks and warped Indian subduction plane: Himalayan Journal of Sciences, v. 2, p. 148–149.

Hermann, J., Rubatto, D., Korsakov, A., and Shatsky, V., 2001, Multiple zircon growth during fast exhumation of diamondiferous, deeply subducted continental crust (Kokchetav Massif, Kazakhstan): Contributions to Mineralogy and Petrology, v. 141, p. 66–82.

Hoskin, P. W. O., 1998, Minor and trace element analysis of natural zircon (ZrSiO4) by SIMS and laser ablation ICPMS: A consideration and comparison of two broadly competitive techniques: Journal of Trace and Microprobe Techniques, v. 16, p. 301–326.

Ireland, T. R., and Williams, I. S., 2003, Considerations in zircon geochronology by SIMS: Reviews in Mineralogy and Geochemistry, v. 53, p. 215–241.

Jain, A. K., Singh, S., Manickavasagam, R. M., Joshi, M., and Verma P. K., 2003, HIMPROBE Programme: Integrated studies on geology, petrology, geochronology and geophysics of the Trans-Himalaya and Karakoram, *in* Mahadevan, T. M., Arora, B. R., and Gupta, K. R., eds., Indian continental lithosphere: Emerging research trends: Geological Society of India Memoirs, no. 53, p. 1–56.

Kaneko, Y., Katayama, I., Yamamoto, H., Misawa, K., Ishikawa, M., Rehman, H. U., Kausar, A. B., and Shiraishi, K., 2003, Timing of Himalayan ultrahigh-pressure metamorphism: Sinking rate and subduction angle of the Indian continental crust beneath Asia: Journal of Metamorphic Geology, v. 21, p. 589–599.

Klootwijk, C. T., Gee, J. S., Peirce, J. W., Smith, G. M., and McFadden, P. L., 1992, An early India-Asia contact: Paleomagnetic constraints from Ninetyeast Ridge, ODP Leg 121, Geology, v. 20, p. 395–398.

Konrad-Schmolke, M., Handy, M. R., Babist, J., and O'Brien, P. J., 2005, Thermodynamic modeling of diffusion-controlled garnet growth: Contributions to Mineralogy and Petrology, v. 16, p. 181–195.

Lacassin, R., Valli, F., Arnaud, N., Leloup, P. H., Paquette, J. L., Haibing, L., Tapponnier, P., Chevalier, M.-L., Guillot, S., Maheo, G., and Zhiqin, X., 2004, Large-scale geometry, offset and kinematic evolution of the Karakorum fault, Tibet: Earth and Planetary Science Letters, v. 219, p. 255–269.

Leech, M. L., Singh, S., Jain, A. K., Klemperer, S. L., and Manickavasagam, R. M., 2005, The onset of India-Asia continental collision: Early, steep subduction required by the timing of UHP metamorphism in the western Himalaya: Earth and Planetary Science Letters, v. 234, p. 83–97.

Leech, M. L., Singh, S., Jain, A. K., Klemperer, S. L., and Manickavasagam, R. M., 2006a, Reply to comment by P. J. O'Brien on "The onset of India-Asia continental collision: Early steep subduction required by the timing of UHP metamorphism in the western Himalaya," Earth and Planetary Science Letters, 234 (2005), 83–97: Earth and Planetary Science Letters, v. 245, p. 817–820.

Leech, M. L., Webb, L. E., and Yang, T. N., 2006b, Diachronous histories for the Dabie-Sulu orogen from high-temperature geochronology, *in* Hacker, B. R., McClelland, W. C., and Liou, J. G., eds., Ultrahigh-pressure metamorphism: Deep continental subduc-

tion: Geological Society of America Special Paper 403 [doi: 10/1130/2006.2403(01)].

Leech, M. L., and Willingshofer, E., 2004, Thermal modeling of the UHP Maksyutov Complex in the south Urals: Earth and Planetary Science Letters, v. 226, p. 85–99.

Liu, F., Xu, Z., Liou, J. G., and Song, B., 2004, SHRIMP U-Pb ages of ultrahigh-pressure and retrograde metamorphism of gneisses, south-western Sulu terrane, eastern China: Journal of Metamorphic Geology, v. 22, p. 315–326.

Ludwig, K. R., 1999, Using Isoplot/Ex, Version 2.01: A geochronological toolkit for Microsoft Excel: Berkeley, CA, Berkeley Geochronology Center Special Publication no. 1a, 47 p.

Massonne, H.-J., and O'Brien, P. J., 2003, The Bohemian massif and the NW Himalaya: EMU Notes in Mineralogy, v. 5, p. 145–187.

McClelland, W. C., Power, S. E., Gilotti, J. A., Mazdab, F. K., and Wopenka, B., in press, U-Pb SHRIMP geochronology and trace-element geochemistry of coesite-bearing zircons, north-east Greenland Caledonides, *in* Cloos, M., Carlson, B., Gilbert, C., Liou, J. G., and Sorenson, S., eds., Convergent margin terranes and associated regions: a volume in honor of W.G. Ernst: Geological Society of America Special Paper.

McDonough, W. F., and Sun, S.-S., 1995, The composition of the Earth: Chemical Geology, v. 120, p. 223–253.

McDougall, I., and Harrison, T. M., 1999, Geochronology and thermochronology by the $^{40}Ar/^{39}Ar$ method: New York, NY, Oxford University Press, 269 p.

Mezger, K., Essene, E. J., and Halliday, A. N., 1992, Closure temperature of the Sm-Nd system in metamorphic garnets: Earth and Planetary Science Letters, v. 113, p. 397–409.

Mukherjee, B. K., and Sachan, H. K., 2003, Carbonate-bearing UHPM rocks from the Tso-Morari region, Ladakh, India: Petrological implications: International Geology Review, v. 45, p. 49–69.

Pognante, U., and Spencer, D. A., 1991, First record of eclogitization from the high Himalayan belt, Kaghan valley (northern Pakistan): Europearn Journal of Mineralalogy, v. 3, p. 613–618.

Powell, R., and Holland, T. J. B., 1988, An internally consistent thermodynamic dataset with uncertainties and correlations. 3. Applications to geobarometry, worked examples, and a computer program: Journal of Metamorphic Geology, v. 6, p. 173–204.

Rubatto, D., 2002, Zircon trace element geochemistry: Partitioning with garnet and the link between U-Pb ages and metamorphism: Chemical Geology, v. 184, p. 123–138.

Rubatto, D., and Hermann, J., 2003, Zircon formation during fluid circulation in eclogites (Monviso, western Alps): Implications for Zr and Hf budget in subduction zones: Geochimica et Cosmochimica Acta, v. 67, p. 2173–2187.

Sachan, H. K., Mukherjee, B. K., Ogasawara, Y., Maruyama, S., Ishida, H., Muko, A., and Yoshioka, N., 2004, Discovery of coesite from Indus suture zone (ISZ), Ladakh, India: Evidence for deep subduction, European Journal of Mineralogy, v. 16, p. 235–240.

Sachan, H. K., Mukherjee, B. K., Ogasawara, Y., Maruyama, S., Pandey, K., Muko, A., Yoshika, N., and Ishada, H., 2001, New discovery of coesite from the Indian Himalaya, *in* Fluid/slab/mantle interactions and ultrahigh-P minerals: Ultrahigh pressure metamorphism workshop 2001: Tokyo, Japan, Waseda University Press, p. 124–128.

Scherer, E. E., Cameron, K. L., and Blichert-Toft, J., 2000, Lu-Hf garnet geochronology: Closure temperature relative to the Sm-Nd system and the effects of trace mineral inclusions: Geochimica et Cosmochimica Acta, v. 64, p. 3413–3432.

Scherer, E., Mezger, K., and Münker, C., 2003, Dating metamorphism with the Lu-Hf garnet method [abs.]: Geophysical Research Abstracts, v. 5, p. 7582.

Schlup, M., Carter, A., Cosca, M., and Steck, A., 2003, Exhumation history of eastern Ladakh revealed by $^{40}Ar/^{39}Ar$ and fission-track ages: the Indus River-Tso Morari transect, NW Himalaya: Journal of the Geological Society of London, v. 160, p. 385–399.

Singh, S., and Jain, A. K., 2003, Himalayan granitoids, *in* Singh, S., ed., Granitoids of Himalayan collisional belt: Journal of the Virtual Explorer, v. 11, p. 1–20.

Srikantia, S. V., and Bhargava, O. N., 1976, Tectonic evolution of the Himachal Himalaya: Tectonics and Metallogeny of South and East Asia: Geological Survey of India Miscellaneous Publication 34, p. 217–236.

Webb, L. E., Leech, M. L., and Yang, T. N., 2006, $^{40}Ar/^{39}Ar$ thermochronology of the Sulu terrane: Late Triassic exhumation of high and ultrahigh-pressure rocks and other implications for Mesozoic tectonics in East Asia, *in* Hacker, B. R., McClelland, W. C., and Liou, J. G., eds., Ultrahigh-pressure metamorphism: Deep continental subduction: Geological Society of America Special Paper 403, [doi: 10/1130/2006.2403(01)].

Williams, I. S., 1998, U-Th-Pb geochronology by ion microprobe, *in* McKibben, M. A., Shanks, W. C., III, and Ridley, W. I., eds., Applications of microanalytical techniques to understanding mineralizing processes: Reviews in Economic Geology, v. 7, p. 1–35.